SSCL-Preprint-2

Superconducting Super Collider Laboratory

SSCL-Preprint-2

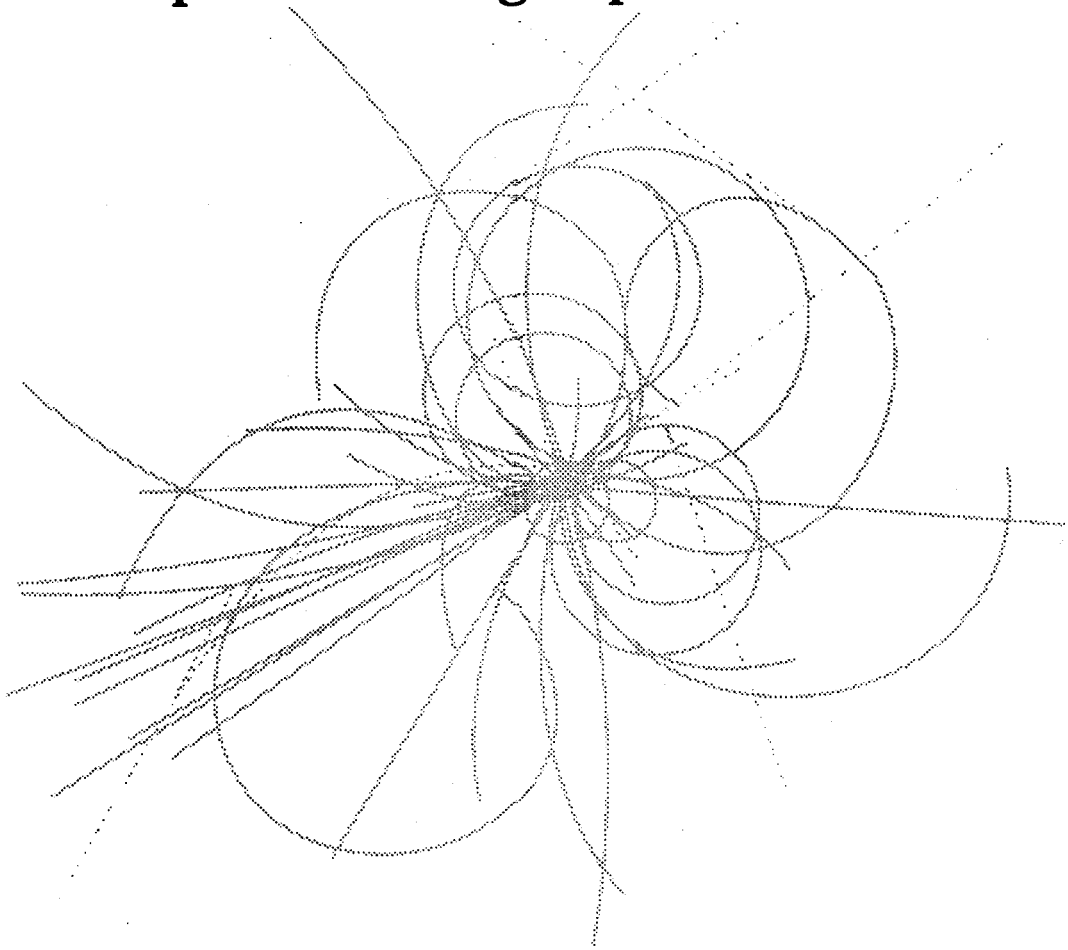

Direct Simulation of Beam Density Evolution in Phase Space: Preliminary Modeling in One Degree of Freedom

S.K. Dutt, J.A. Ellison, T. Garavaglia, S.K. Kauffmann, T. Sen, M.J. Syphers, and Y.T. Yan

October 1991

To be published by American Institute of Physics. SSCL-Preprint-2

Direct Simulation of Beam Density Evolution in Phase Space: Preliminary Modeling in One Degree of Freedom*

S.K. Dutt, J.A. Ellison, T. Garavaglia, S.K. Kauffmann,
T. Sen, M.J. Syphers, and Y.T. Yan

Accelerator Design and Operations Division
Superconducting Super Collider Laboratory†
2550 Beckleymeade Avenue
Dallas, TX 75237

October 1991

* Presented at the Advanced Beam Dynamics Workshop on Effects of Errors in Accelerators, Their Diagnosis and Corrections, Corpus Christi, Texas, October 3–8, 1991.

† Operated by the Universities Research Association, Inc., for the U.S. Department of Energy under Contract No. DE-AC35-89ER40486.

Direct Simulation of Beam Density Evolution in Phase Space: Preliminary Modeling in One Degree of Freedom

S.K. Dutt, J.A. Ellison, T. Garavaglia, S.K. Kauffmann, T. Sen, M.J. Syphers, and Y.T. Yan
Superconducting Super Collider Laboratory,* Dallas, TX 75237

Abstract

The concept of phase space density provides a properly macroscopic description of a beam bunch of mutually non-interacting particles. Ideally, simulations of particle beam behavior ought to concentrate directly on the dynamics of the beam phase space density rather than on that of individual particles—an immediate benefit being the elimination of the statistical uncertainty inevitably arising from the sampling of such particles. Here a preliminary step is taken in the direction of this desirable goal—a "toy" one-degree-of-freedom (the transverse horizontal) beam phase space density is simulated for a highly simplified lattice consisting of a purely linear FODO ring which contains a single thin-element nonlinear kick. These meager ingredients produce a fascinating collection of beam density snapshots in the phase space—including such phenomena as the filamentation and "fragmentation" of a kicked beam, the process of formation of phase space islands under a variety of circumstances, and spiral twisting of the beam density within the dynamic aperture.

1.0 Introduction and Basic Concepts

Particle beam evolution simulations have heretofore largely focused on the tracking of a relatively small number of individual particles. Particle beams are, however, macroscopic, not microscopic, objects, containing upwards of 10^8 particles in each bunch, which are therefore more satisfactorily described by their density in phase space. Below we briefly develop the basic concepts, formalism, and dynamical equations associated with particle beam density in phase space for mutually non-interacting particles in the restricted context of a single transverse degree of freedom (the formulas generalize straightforwardly to the more realistic case of three degrees of freedom). In the next section the results of highly simplified, but surprisingly result-rich simulations which apply these concepts are presented.

Consider a particle beam consisting of N discrete, mutually non-interacting particles, whose motion we propose to study in only the horizontal transverse degree of freedom. With each such particle we thus associate the pair of phase space co-ordinate $X_i(s)$ and $X_i'(s)$, $i = 1, 2 \cdots, N$. The appropriate definition of the beam phase space density in this case is,

$$\rho_N(x, p, s) \equiv \frac{1}{N} \sum_{i=1}^{N} \delta(x - X_i(s))\delta(p - X_i'(s)). \tag{1}$$

* Operated by the Universities Research Association, Inc., for the U. S. Department of Energy under Contract No. DE-AC35-89ER40486

Note that $\rho_N(x,p,s)$ satisfies the key intuitive requirement that,

$$\iint_R dx\, dp\, \rho_N(x,p,s) = \tag{2}$$

The fraction of the N particles which have their phase space coordinates within R at s, where R is any region of phase space.

This implies in particular that,

$$\int_{-\infty}^{\infty} dx \int_{-\infty}^{\infty} dp\, \rho_N(x,p,s) = 1 \text{ at all } s. \tag{3}$$

The N mutually non-interacting particle phase space co-ordinates $(X_i(s), X_i'(s))$, $i = 1, \cdots, N$, each satisfies Hamilton's equations,

$$\frac{d}{ds}(X_i(s)) = \frac{\partial H(X_i(s), X_i'(s), s)}{\partial X_i'(s)}, \quad i = 1, \cdots, N, \tag{4a}$$

$$\frac{d}{ds}(X_i'(s)) = -\frac{\partial H(X_i(s), X_i'(s), s)}{\partial X_i(s)}, \quad i = 1, \cdots, N, \tag{4b}$$

with the *same* single-particle Hamiltonian function H.

The solutions to Eqs. (4) can be expressed in terms of a single-particle one-to-one symplectic map $(T_{s;s_0}, T'_{s;s_0})$ which carries each of the N particles forward from its initial conditions at $s = s_0$,

$$X_i(s) = T_{s;s_0}[X_i(s_0), X_i'(s_0)], \quad i = 1, \cdots, N, \tag{5a}$$

$$X_i'(s) = T'_{s;s_0}[X_i(s_0), X_i'(s_0)], \quad i = 1, \cdots, N. \tag{5b}$$

It is helpful at this stage to introduce the vector notations $\vec{Z}_i(s) \equiv (X_i(s), X_i'(s))$, $i = 1, \cdots, N$, $\vec{T}_{s;s_0} \equiv (T_{s;s_0}, T'_{s;s_0})$, and $\vec{z} \equiv (x,p)$. We shall now obtain the rule for the evolution of $\rho_N(\vec{z},s)$ from the initial $\rho_N(\vec{z},s_0)$ by substituting Eqs. (5) into the definition (1) of $\rho_N(\vec{z},s)$ and then applying a delta-function identity.

$$\begin{aligned}\rho_N(\vec{z},s) =& \frac{1}{N}\sum_{i=1}^{N} \delta^{(2)}(\vec{z} - \vec{T}_{s;s_0}[\vec{Z}_i(s_0)]) \\ =& \frac{1}{N}\sum_{i=1}^{N} \delta^{(2)}(\vec{T}^{-1}_{s;s_0}[\vec{z}] - \vec{Z}_i(s_0)) \times \text{Jacobian}(\vec{T}^{-1}_{s;s_0}[\vec{z}]).\end{aligned} \tag{6}$$

Because $\vec{T}_{s;s_0}$ is symplectic, $\text{Jacobian}(\vec{T}^{-1}_{s;s_0}[\vec{z}]) = 1$. Referring again to the definition (1) of ρ_N, we see that Eq. (6) implies that,

$$\rho_N(\vec{z},s) = \rho_N(\vec{T}^{-1}_{s;s_0}[\vec{z}], s_0), \tag{7}$$

which is the fundamental rule for the evolution in s of ρ_N. The appearance of the inverse, or "s-reversed", map $\vec{T}^{-1}_{s;s_0}$ in Eq. (7) may strike those accustomed to individual particle tracking as counter-intuitive. Further on in this section we shall, however, be showing that the "counter-intuitive" Eq. (7) is in fact equivalent to the celebrated theorem of Liouville. One can as well obtain the "s-reversed" feature in differential form by taking the partial derivative of $\rho_N(\vec{z},s)$ with respect to s in Eq. (1), and then using Hamilton's equations (4) in conjunction with the properties of δ-functions to obtain,

$$\frac{\partial \rho_N(x,p,s)}{\partial s} = \{H, \rho_N\}_{(x,p)}, \tag{8}$$

where $\{\ \}_{(x,p)}$ is the Poisson bracket with respect to (x,p). Eq. (8) is the Vlasov or Liouville equation for ρ_N, and is formally "s-reversed" from the equation one obtains for a function F of only dynamical variables $(X(s), X'(s))$, the latter being,

$$\frac{d}{ds}(F(X(s), X'(s))) = -\{H, F\}_{(X(s),X'(s))}. \tag{9}$$

It is clear, however, that $\rho_N(x,p,s)$ is a different object from such an $F(X(s), X'(s))$. The Vlasov Eq. (8) is, of course, solved by the fundamental s-evolution Eq. (7).

Our phase space density $\rho_N(\vec{z}, s)$ has a δ-function "spike" at the $\vec{z}$ locations of each of the discrete particle $\vec{Z}_i(s)$, $i = 1, \cdots, N$ (the phase space "fraction" of each such δ-function "spike" is $1/N$). The evolution in s of $\rho_N(\vec{z}, s)$ is thus essentially the evolution of the N individual particle phase space points $\vec{Z}_i(s)$. While this is a conceptually satisfactory state of affairs, it renders simulation of ρ_N impractical because of the extremely large size of N for beam bunches. For practical simulations one needs to deal with a "smoothed" continuous version of phase space density in the limit that N tends to infinity. Such a "smooth" continuous density emerges naturally if one conceives of selecting the initial (injected) $\vec{Z}_i(s_0)$, $i = 1, \cdots, N$, by a random Monte-Carlo process from an underlying smooth probability distribution density $d(\vec{z})$. The essence of the idea behind the Monte-Carlo procedure is that the initial $\rho_N(\vec{z}, s_0)$ thus obtained has the limiting behavior

$$\lim_{A\to 0}\lim_{N\to\infty} \frac{1}{A}\iint\limits_{R_A(\vec{z})} d^2\vec{z}\,'\rho_N(\vec{z}\,', s_0) = d(\vec{z}), \tag{10}$$

where $R_A(\vec{z})$ is a phase space region of "area" A which shrinks toward just the point $\vec{z}$ as $A \to 0$. This result comes under the technical nomenclature of "the law of large numbers".

Given such a Monte-Carlo selection of the initial $\vec{Z}_i(s_0)$, $i = 1, \cdots N$, from the underlying smooth probability density $d(\vec{z})$, one may, for arbitrary s, define a smoothed ρ in the limit $N \to \infty$ as,

$$\text{smoothed } \rho(\vec{z}, s) \equiv \lim_{A\to 0}\lim_{N\to\infty} \frac{1}{A}\iint\limits_{R_A(\vec{z})} d^2\vec{z}\,'\rho_N(\vec{z}\,', s). \tag{11}$$

We can ask how this smoothed ρ evolves with s. Making use of Eq. (7) for the evolution with s of ρ_N, and also the symplecticity of $\vec{T}_{s;s_0}$, we obtain,

$$\text{smoothed } \rho(\vec{z}, s) = \lim_{A\to 0}\lim_{N\to\infty} \frac{1}{A}\iint\limits_{R_A(\vec{z})} d^2\vec{z}\,'\rho_N(\vec{z}\,', s) \tag{12a}$$

$$= \lim_{A\to 0}\lim_{N\to\infty} \frac{1}{A}\iint\limits_{R_A(\vec{z})} d^2\vec{z}\,'\rho_N(\vec{T}^{-1}_{s;s_0}[\vec{z}\,'], s_0) \tag{12b}$$

$$= \lim_{A\to 0}\lim_{N\to\infty} \frac{1}{A}\iint\limits_{\vec{T}^{-1}_{s;s_0}[R_A(\vec{z})]} d^2\vec{w}\,\rho_N(\vec{w}, s_0). \tag{12c}$$

At this point we again make use of the symplecticity of $\vec{T}_{s;s_0}$ to assert that the phase space "area" of the image region $\vec{T}^{-1}_{s;s_0}[R_A(\vec{z})]$ is A. Further, since $R_A(\vec{z})$ shrinks toward just the point $\vec{z}$ as $A \to 0$, the image region $\vec{T}^{-1}_{s;s_0}[R_A(\vec{z})]$ must perforce shrink toward just the point $\vec{T}^{-1}_{s;s_0}[\vec{z}]$ as $A \to 0$. Thus, from Eq. (12c) and Eq. (10), we have that,

$$\text{smoothed } \rho(\vec{z}, s) = d(\vec{T}^{-1}_{s;s_0}[\vec{z}]) \tag{13a}$$

$$= \text{smoothed } \rho(\vec{T}^{-1}_{s;s_0}[\vec{z}], s_0), \tag{13b}$$

where Eq. (13b) follows from Eqs. (10) and (11). Eq. (13b) is our principal result, i.e.,that the smoothed ρ obeys exactly the same fundamental rule for evolution in s as does the "spiky" ρ_N, namely Eq. (7). Eq. (13a) makes explicit the nature of smoothed $\rho(\vec{z}, s)$ at any s in terms of the smooth probability distribution density $d(\vec{z})$ underlying the Monte-Carlo selection of the initial (injected) $\vec{Z}_i(s_0)$, $i = 1, \cdots, N$. With smoothed ρ in hand, one has passed to a truly macroscopic description of the beam.

We wind up this section with a brief demonstration that Eq. (7) (or Eq. (13b)), in which the "counter-intuitive" s-reversed map $\vec{T}^{-1}_{s;s_0}$ appears, is, in fact, equivalent to Liouville's theorem.

Liouville's theorem doesn't directly deal with our $\rho(\vec{z}, s)$, but rather makes an assertion about the character of $\rho(\vec{z}, s)$ when it is evaluated at the z-value of an arbitrary beam particle trajectory at s. Let this arbitrary beam particle trajectory be denoted $\vec{Z}(s)$. Then the "co-moving" phase space density of the Liouville theorem is defined as $\rho(\vec{Z}(s), s)$. Since $\vec{Z}(s)$ is some permitted beam particle trajectory, it must satisfy,

$$\vec{Z}(s) = \vec{T}_{s;s_0}[\vec{Z}(s_0)]. \tag{14}$$

Now we apply equations (7) and (14) in sequence to our "co-moving" $\rho(\vec{Z}(s), s)$ to obtain,

$$\begin{aligned} \rho(\vec{Z}(s), s) &= \rho(\vec{T}^{-1}_{s;s_0}[\vec{Z}(s)], s_0) \\ &= \rho(\vec{T}^{-1}_{s;s_0}[\vec{T}_{s;s_0}[\vec{Z}(s_0)]], s_0) \\ &= \rho(\vec{Z}(s_0), s_0), \end{aligned} \tag{15}$$

i.e., any "co-moving" phase space density $\rho(\vec{Z}(s), s)$ does not vary with s. This is the theorem of Liouville.

Conversely, let us assume Liouville's theorem, and see if we can obtain the "counter-intuitive" Eq. (7). The Liouville theorem asserts that

$$\rho(\vec{z}, s) = \rho(\vec{z}_0, s_0), \tag{16}$$

where $\vec{z}$ is the phase space location at s of a beam particle that was at phase space location $\vec{z}_0$ at $s = s_0$. Thus,

$$\vec{z} = \vec{T}_{s;s_0}[\vec{z}_0], \tag{17a}$$

which implies that,

$$\vec{z}_0 = \vec{T}^{-1}_{s;s_0}[\vec{z}]. \tag{17b}$$

If we substitute Eq. (17b) into the right hand side of Eq. (16), we obtain the "counter-intuitive" Eq. (7). This completes the demonstration that Eq. (7) (and thus also the Vlasov equation (8)) is equivalent to Liouville's theorem.

We hasten to point out that the "co-moving" phase space density $\rho(\vec{Z}(s), s)$ of the Liouville theorem is of no direct interest in the simulation of beam evolution, as $\rho(\vec{Z}(s), s)$ does not evolve at all with s. The interesting quantity to compute is our fixed point phase space density $\rho(\vec{z}, s)$, which evolves according to Eq. (7).

2.0 Simulation Results from a Simple Model

Evolution of beam phase space density in a single transverse (horizontal) degree of freedom was simulated at the center of a focusing quadrupole of an extremely simple lattice. The beam was injected at this point and then passed through a linear FODO lattice back around to this point (a 2x2 transfer matrix characterized by a nominal fractional tune and the focusing quad beta value was used to simulate this portion of the beam's journey), where it was subjected to a non-linear kick which could be selected as a thin-element sextupole, octupole, or decapole—or

some combination of these. Multiple turns through this "toy" lattice were simulated, starting from initial (injected) smoothed phase space densities of the Gaussian form,

$$\rho(x,p,s=0) = \left(\frac{\beta}{2\pi\sigma^2}\right) \exp\left(-\left(\frac{(x-x_0)^2+\beta^2(p-p_0)^2}{2\sigma^2}\right)\right). \tag{18}$$

Such an initial ρ will, of course, be invariant if the non-linear kick is chosen to be zero and the "off-center" parameters x_0 and p_0 are as well chosen to be zero.

As the s-evolution of ρ is governed by Eq. (7) (or Eq. (13b)), the resultant ρ after n turns may be formally written as,

$$\rho(\vec{z}, s=nC) = \rho(\vec{T}^{-1}_{nC;0}[\vec{z}], s=0), \tag{19}$$

where C is the machine circumference. The appearance of the "s-reversed" n-turn map $\vec{T}^{-1}_{nC;0}$ in Eq. (19) implies that we must use the *negative* of the conventional (i.e., for individual particle evolution) nonlinear kick *followed* by the *inverse* of the conventional 2x2 FODO transfer matrix. The correct details of such s- reversal demand attentiveness and care on the part of the programmer accustomed to simulating individual particle evolution. The penalty for not getting the details of s-reversal right is normally a rather trivial error in the orientation of the phase space density (e.g., an "off center" beam with fractional tune between zero and one-half would turn-by-turn circulate anti-clockwise instead of clockwise around the phase space if one neglected to invert the conventional FODO transfer matrix). In one instance, however, a much more severe penalty for neglecting an aspect of s-reversal was encountered. It was decided to look at the effect of slowly and smoothly ramping the nonlinear kick up to its final strength over many turns, in contrast to its being present at its full strength from injection. Of course, if one s-reverses a gentle, smooth *initial* ramp-*up*, one gets a gentle, smooth *final* ramp-*down*. Ignoring this aspect of s-reversal produced grossly wrong results.

For the graphical representation of the simulated ρ, it is convenient to change its independent phase space variables from (x,p) to the "β-scaled" $(x,\beta p)$. Then the injected phase space density (18) becomes just a (possibly) off-center Gaussian of rotation, whose contour lines are circles. To plot ρ, we lay down a square grid of K^2 square cells, centered on $(x=0, \beta p=0)$. The grid typically has a side length of several σ, so that it covers the phase space region of significant injected beam density. We compute the n-turn ρ, in accord with Eq. (19), at each of the $(K+1)^2$ nodes of our square grid, and then plot the resulting 3-D surface and/or its contour lines.

Since we compute, i.e., essentially track in reverse s, the phase space density at $(K+1)^2$ nodes, one might wonder if it would be just as well to track $(K+1)^2$ individual particles in the conventional fashion. Indeed, we know that if we Monte-Carlo select the initial (injected) phase space co-ordinates for these particles according to the initial ρ of Eq. (18), then as the number of particles thus selected goes to infinity, we can in principle obtain the n-turn ρ of Eq. (19) by the smoothing process of Eq. (11). Of course, it is not a viable proposition to track an infinite number of individual particles. In case the number is finite, the "smoothing region" $R_A(\vec{z})$ of Eq. (11) must encompass enough of these particles to reduce the statistical uncertainty to a tolerable level. If, for example, $R_A(\vec{z})$ contains only one such particle, the statistical uncertainty is an intolerable 100%. One hundred particles in $R_A(\vec{z})$, for a statistical uncertainty of around 10%, would probably be considered tolerable. So the phase space density resolution one could achieve by tracking a finite number of individual particles would be defined by phase space regions containing around 100 particles each. These regions of threshhold resolvability would be much larger where the phase space density was small than where it was large.

The above state of affairs for individual particle tracking contrasts sharply with our direct phase space simulation on the $(K+1)^2$ nodes of our square grid of K^2 square cells. Our regions of threshhold resolvability are just the square cells themselves, which are of uniform size throughout our grid. We track only $(K+1)^2/K^2 \approx 1$ node points per resolvable cell. Unlike

the situation with individual particles whose initial conditions are selected by a Monte-Carlo process, our precise initial ρ values at the node points can propagate no statistical uncertainty whatsoever. The bottom line is that we naturally achieve a uniform resolution throughout our square grid, irrespective of variations in the value of ρ over that region, and that we achieve that resolution by tracking about one node point per resolved cell—with no statistical uncertainty whatsoever, rather than about 100 individual particles per resolved region, with about a 10% statistical uncertainty.

It is no wonder then, that the phase space density plots we display below reveal some interesting details which individual particle tracking cannot practically resolve.

Figure 1 is a sequence of contour plots of ρ showing the progression with turn number of the phase space density from a centered Gaussian of revolution to a sharply delineated triangular region (the separatrix) which bounds the dynamic aperture in the presence of just the sextupole kick at a fractional tune very close to $\frac{1}{3}$. Figure 2 shows the corresponding sequence of 3-D surface plots. Here we see that within the triangular dynamic aperture, the phase space density is being twisted into a progressively tighter spiral shape with increasing turn number—a subtle effect that eventually runs into the limit of our grid resolution, and would be virtually impossible to see with workaday individual particle tracking. Figure 3 shows that this spiral twisting is eliminated when the sextupole is adiabatically ramped (a smooth quadratic spline shape was used for the ramp) up to its full strength over the first 1000 turns. The contour lines within the triangular dynamic aperture then assume the rounded triangular shapes characteristic of individual particle trajectories under these circumstances.

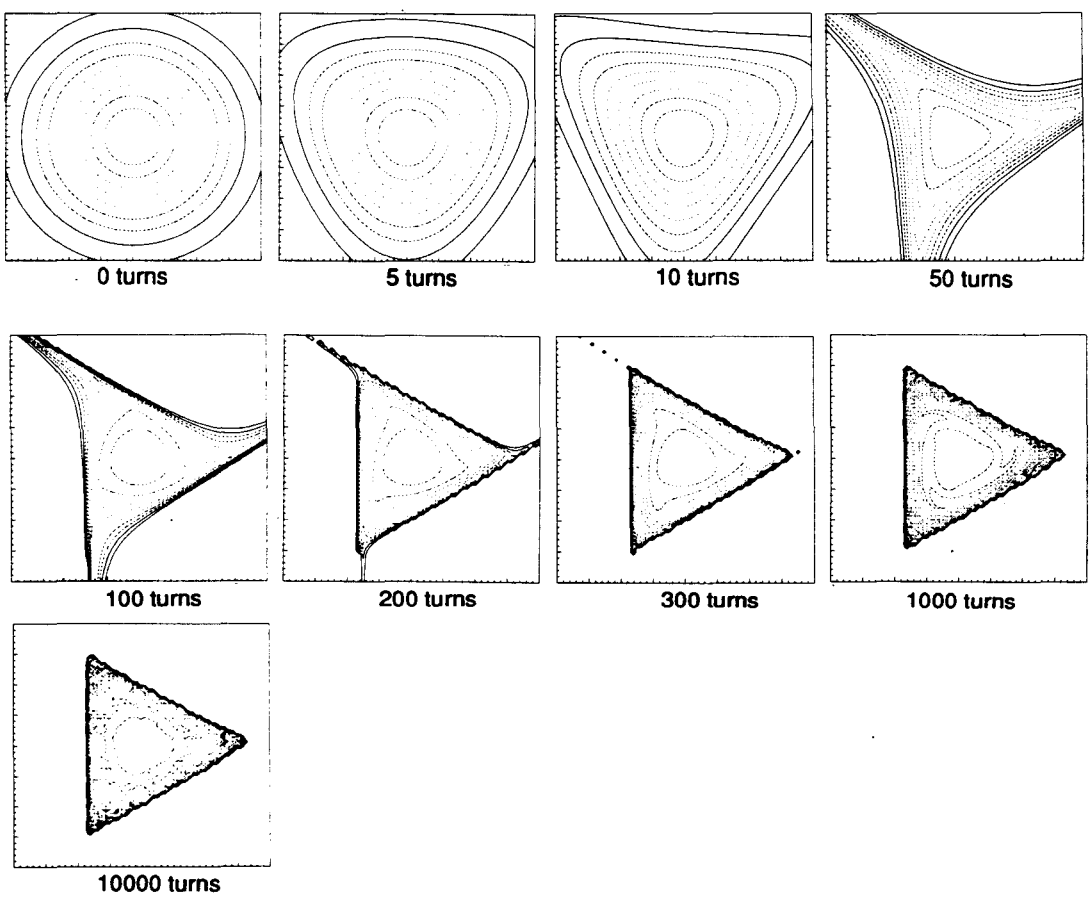

Figure 1. Contour plots for sextupole only with tune near $\frac{1}{3}$ (0.336666667).

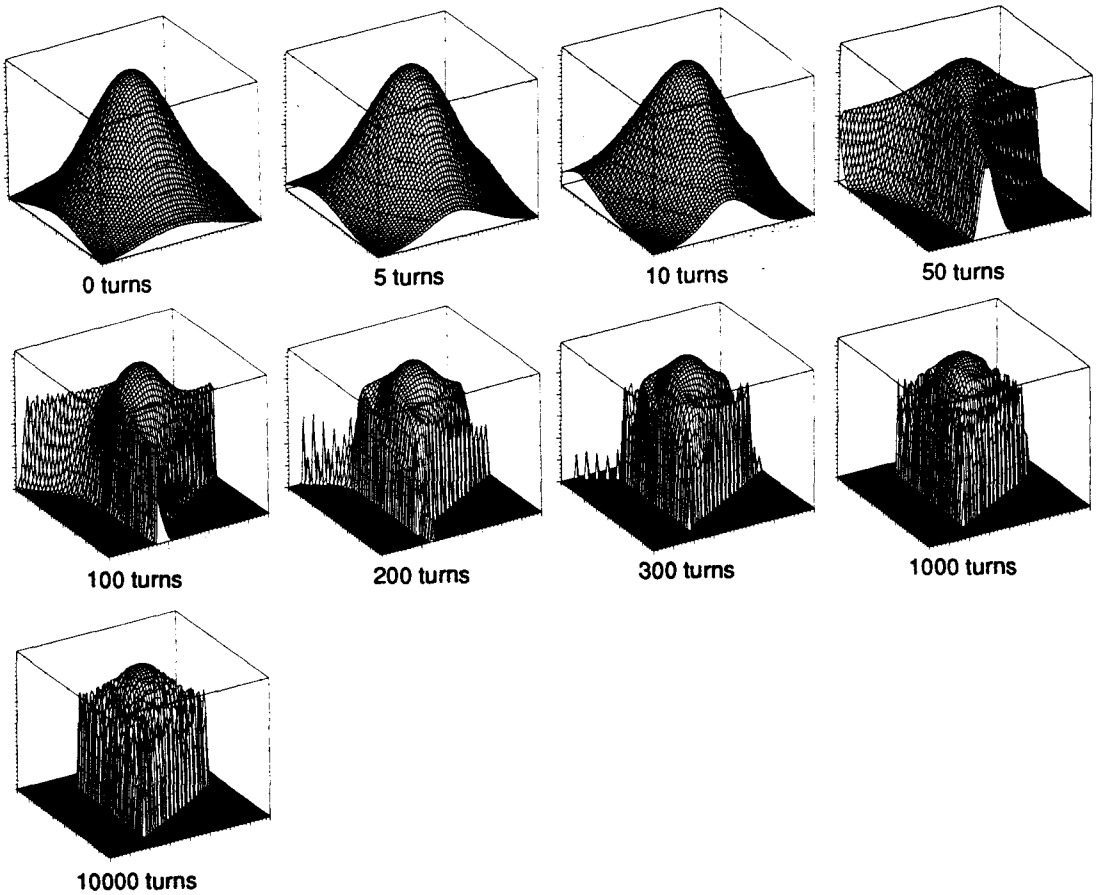

Figure 2. 3-D plots for sextupole only with tune near $\frac{1}{3}$ (0.336666667).

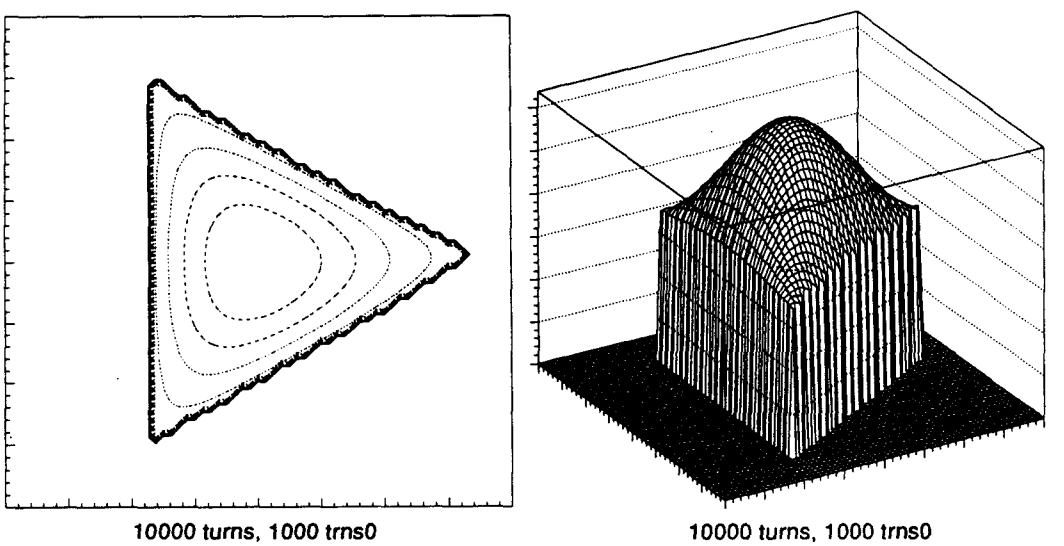

Figure 3. Same as 10,000-turn cases in Figures 1 and 2, except that the sextupole is ramped adiabatically from zero to its full strength over the first 1000 turns.

Figure 4 is a sequence of contour plots of ρ for the same lattice parameters as Figures 1 and 2, but here a much narrower beam is injected well off-center. Because the tune is near $\frac{1}{3}$, this beam travels clockwise around the phase space by about 120^0 per turn. Due to the presence of the sextupole, this circulating beam begins to elongate away from its initial Gaussian shape. Indeed, the beam is pulled like a strand of taffy, and that strand, continuing to elongate, begins to conform approximately to part of a triangular outline. As the elongation continues, the "tail" of the "taffy" begins to "fragment", and the triangular outline tends to spiral somewhat inwards. Ultimately, this elongating, spiraling outline disintegrates completely into "fragments" which occupy a triangular annulus. This is quite a nice simulation of the filamentation and "fragmentation" process for beams "kicked" off center. Figure 5 shows one stage of the filamentation-triangularization-"fragmentation" process in 3-D.

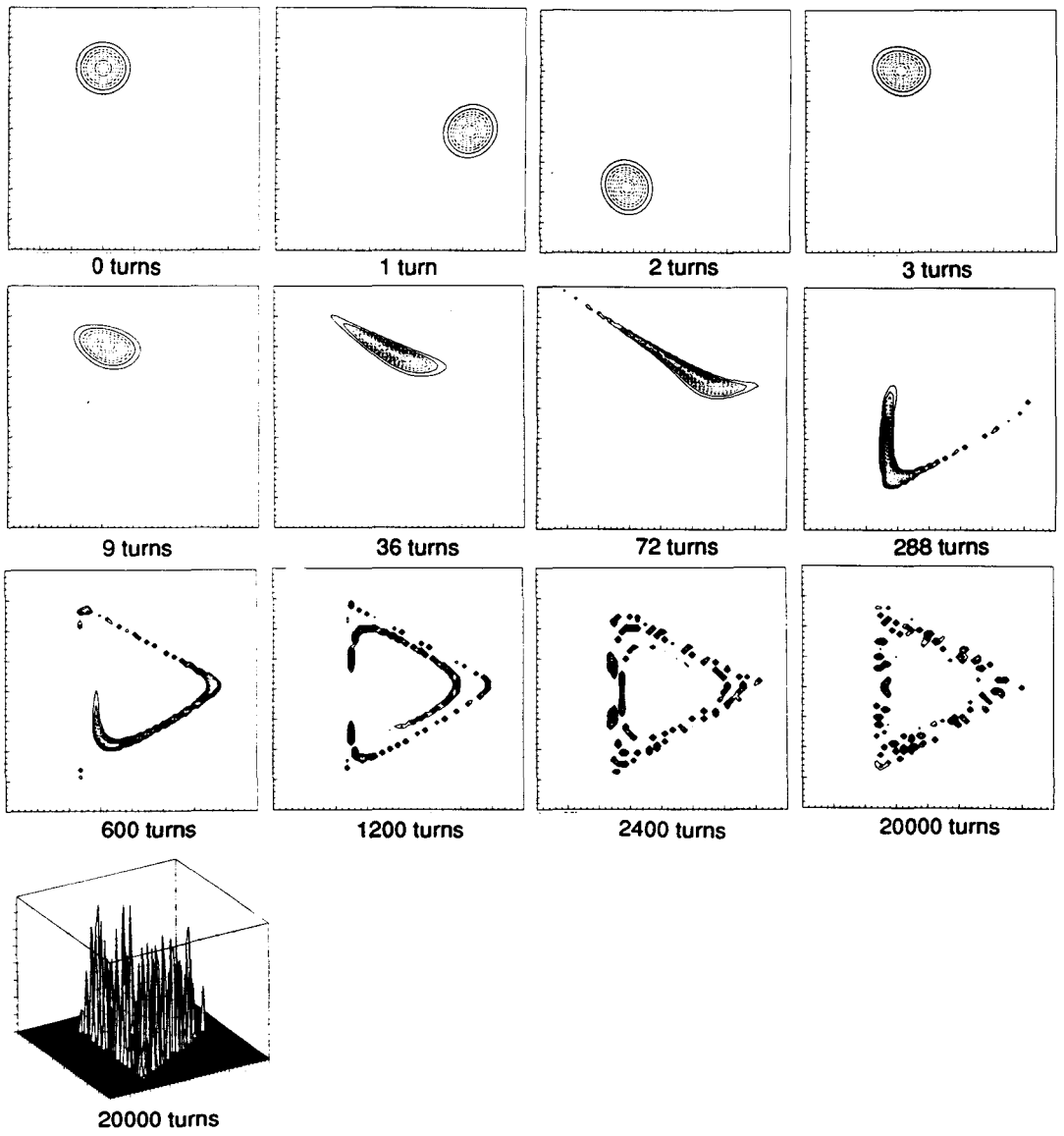

Figure 4. Same as Figure 1, except that here a much narrower beam is injected well off-center. Note progressive filamentation-"fragmentation" of this "kicked" beam.

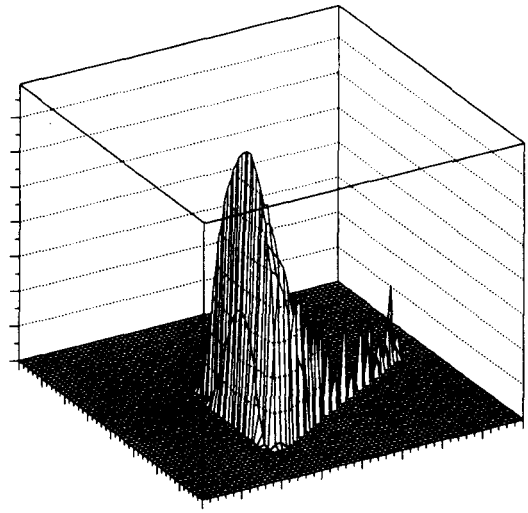

Figure 5. 3-D plot of the 288-turn stage of filamentation from the contour plot turn-series of Figure 4.

If we now change the tune to be near $\frac{1}{4}$ and simultaneously boost the sextupole strength in order to keep the dynamic aperture on the same grid, we get the progression of contour plots in Figure 6. The dynamic aperture takes many more turns to "settle down" than in Figure 1, but its form is worth the wait. Instead of being a triangle, the aperture consists of a central square region ringed by four well-separated islands. Figure 7 shows this configuration in 3-D. Figure 8 shows that a 900-turn adiabatic ramp-up of the sextupole doesn't permit the islands to form—the dynamic aperture is reduced to just the central square region.

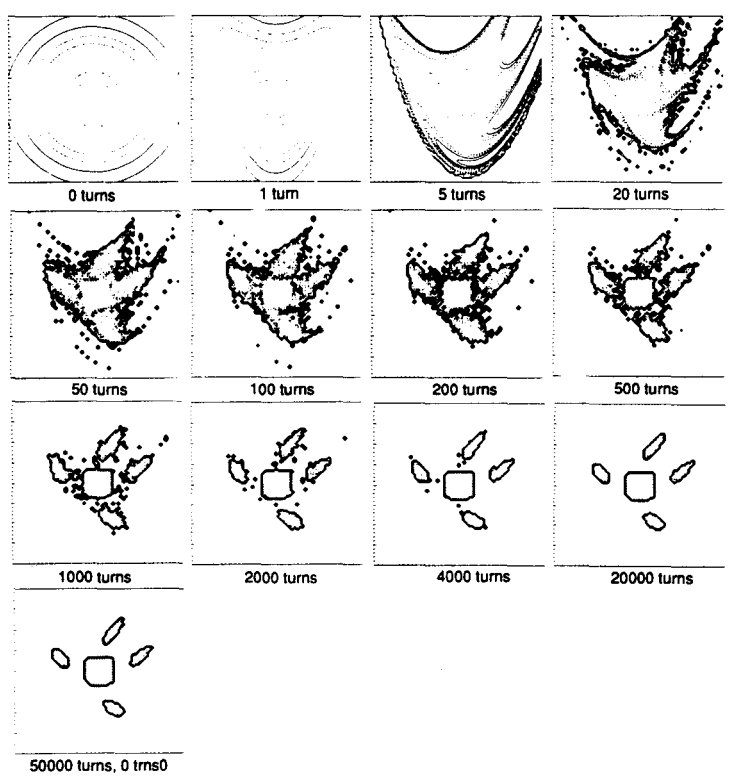

Figure 6. Contour plots for sextupole only with tune near $\frac{1}{4}$ (0.255).

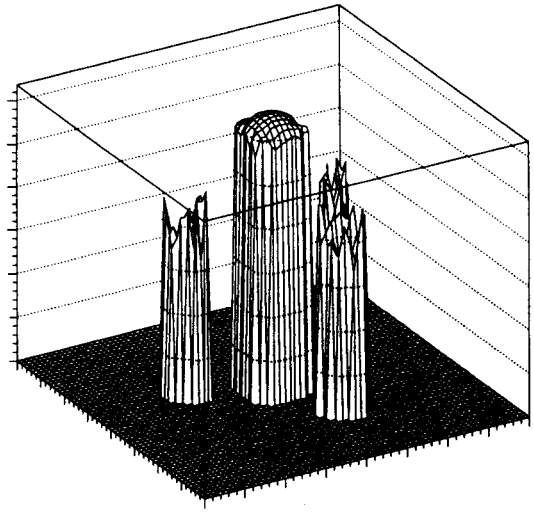

50000 turns, 0 trns0

Figure 7. 3-D plot of the 50,000-turn stage of stable island formation from the contour plot turn-series of Figure 6.

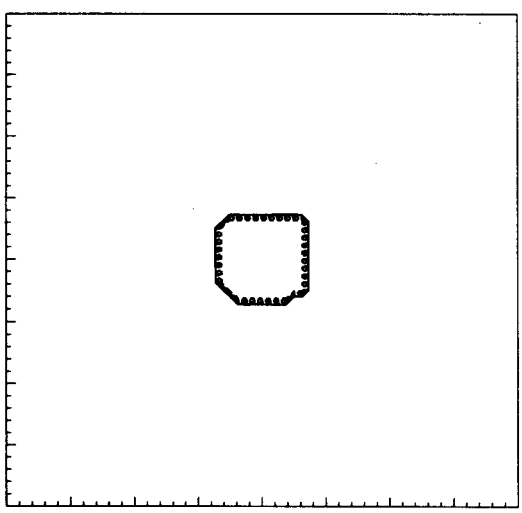

50000 turns, 900 trns0

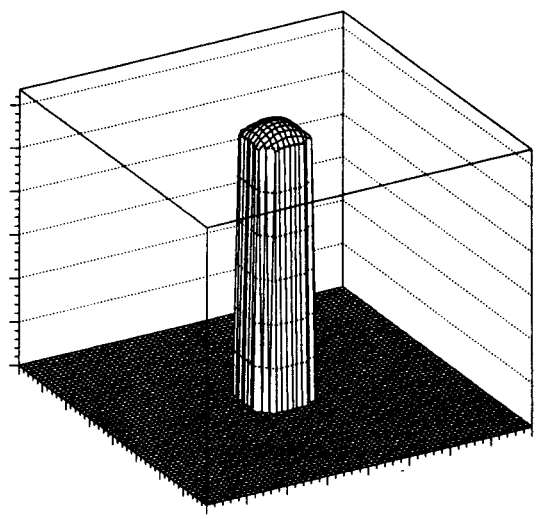

50000 turns, 900 trns0

Figure 8. Same as the 50,000-turn stage of Figures 6 and 7, except that the sextupole is ramped up adiabatically over the first 900 turns. Islands fail to form.

We now move the tune upwards from near $\frac{1}{4}$ to near 0.283, a value close to that proposed for the SSC. Adding an octupole to the sextupole once again produces four islands ringing a "mainland" which roughly mixes some attributes of square and triangle, as shown in the contour plot progression of Figure 9. Figure 10 shows this configuration in 3-D. These islands are surprisingly robust—a 1000-turn adiabatic ramp-up of the sextupole-octupole combination diminishes their height without eliminating them, as shown in Figure 11.

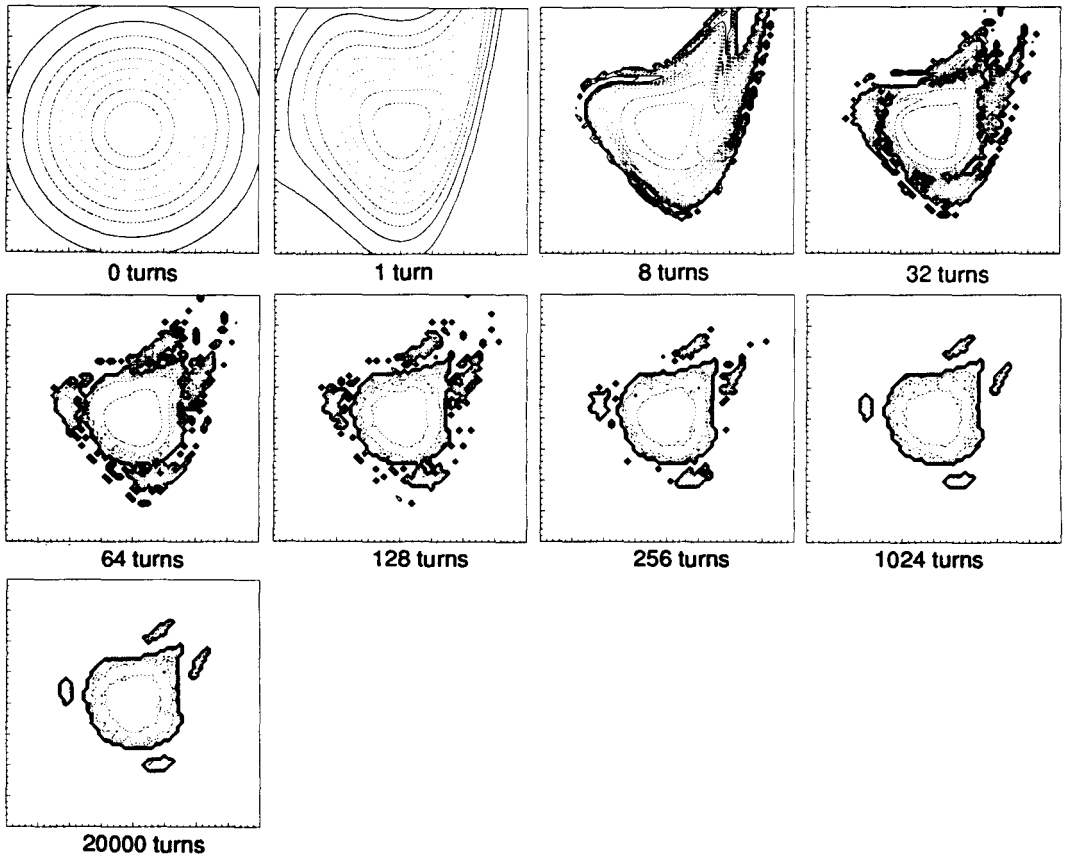

Figure 9. Contour plots for sextupole combined with octupole for tune near 0.283 (0.283141592654).

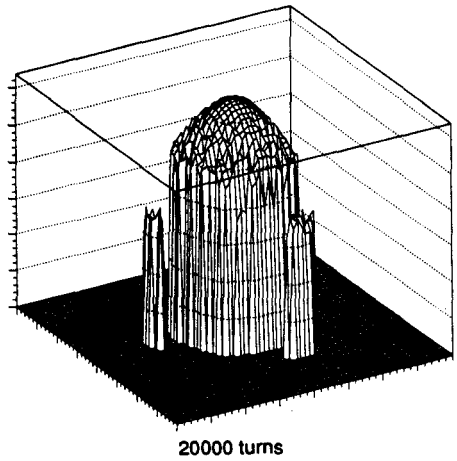

Figure 10. 3-D plot of the 20,000-turn stage of stable island formation from the contour plot turn-series of Figure 9.

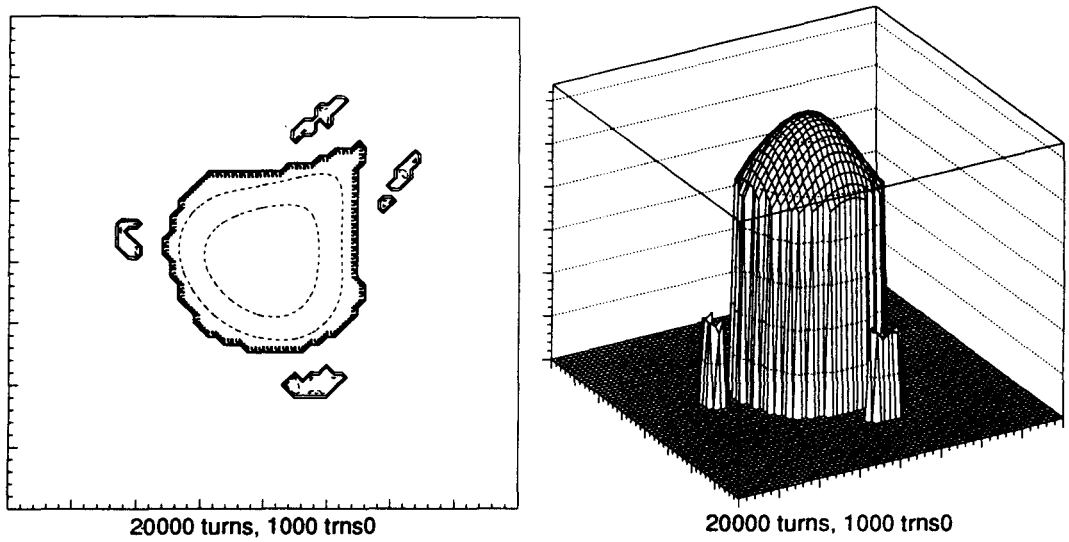

Figure 11. Same as the 20,000-turn stage of Figures 9 and 10, except for adiabatic ramp-up of the nonlinear kick over the first 1000 turns. Islands are merely diminished in height here.

Going back now to the sextupole alone, and moving the tune to somewhat above $\frac{1}{5}$ (0.221), we see in Figure 12 a crop of five islands ringing a mainland which is a rough hybred of pentagon and triangle. Figure 13 shows that these islands fail to form when the sextupole is adiabatically ramped up over 900 turns.

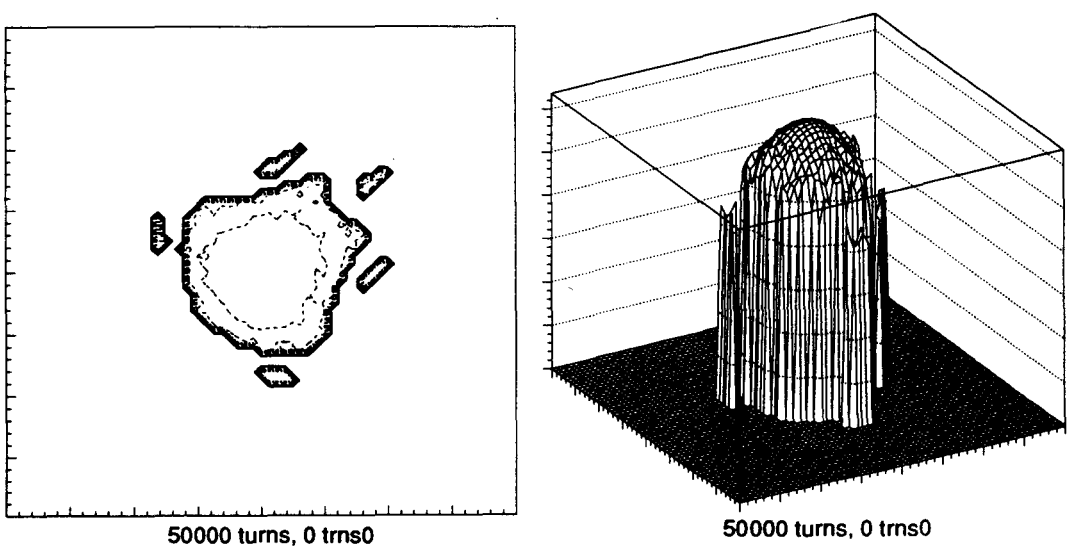

Figure 12. Sextupole only with tune near $\frac{1}{5}$ (0.221).

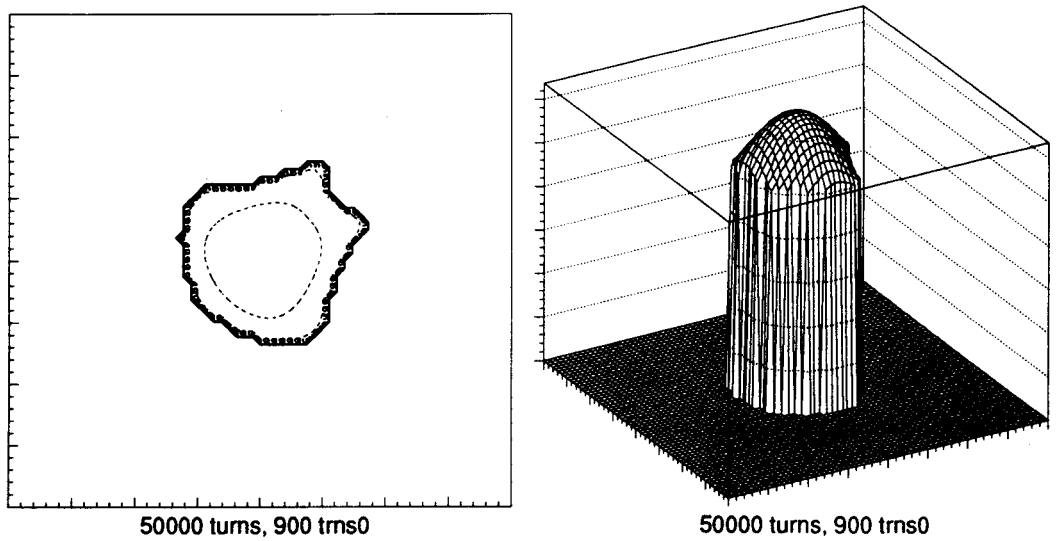

Figure 13. Same as Figure 12 except for 900-turn adiabatic sextupole ramp-up.

Figure 14 shows five less well-separated islands at a tune somewhat above $\frac{2}{5}$ (0.4325). Figure 15 shows their elimination by the 900-turn adiabatic ramp-up.

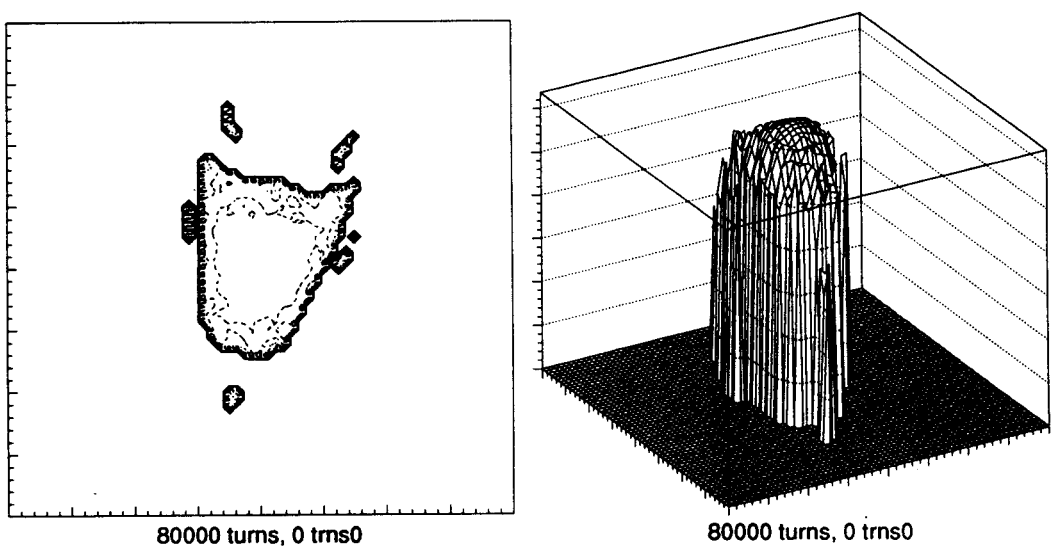

Figure 14. Sextupole only with tune near $\frac{2}{5}$ (0.4325).

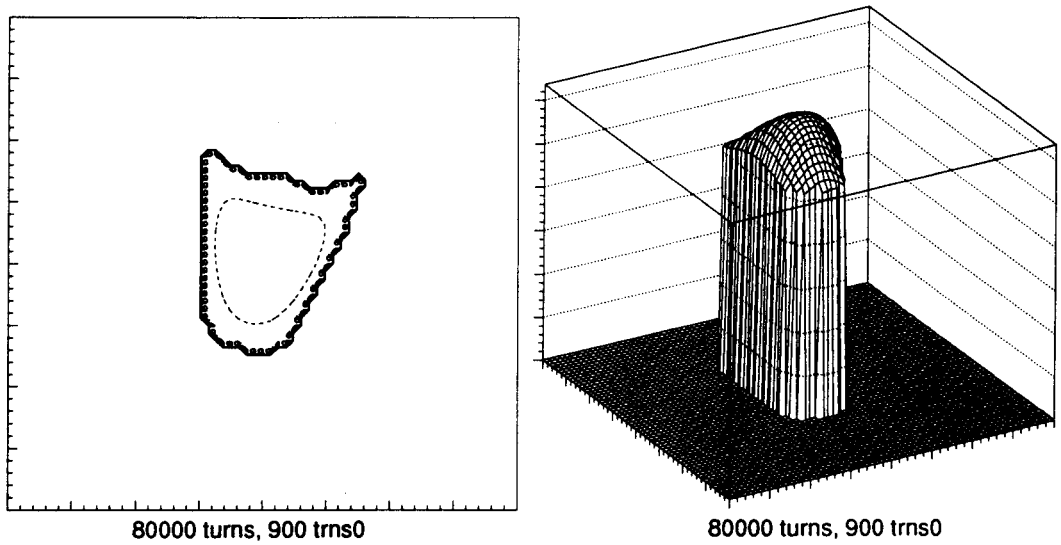

Figure 15. Same as Figure 14 except for 900-turn adiabatic sextupole ramp-up.

Figure 16 is a delicately chosen combination of sextupole, octupole, and beta at a tune just above $\frac{1}{3}$ (0.34), which is known to produce some very long, looping closed particle orbits well beyond the purely sextupole triangular apertune. Three fat blobs appear at a substantial distance from the triangle at the center. Figure 17 shows that these blobs also largely vanish when the sextupole and octupole are put through a 900-turn adiabatic ramp-up.

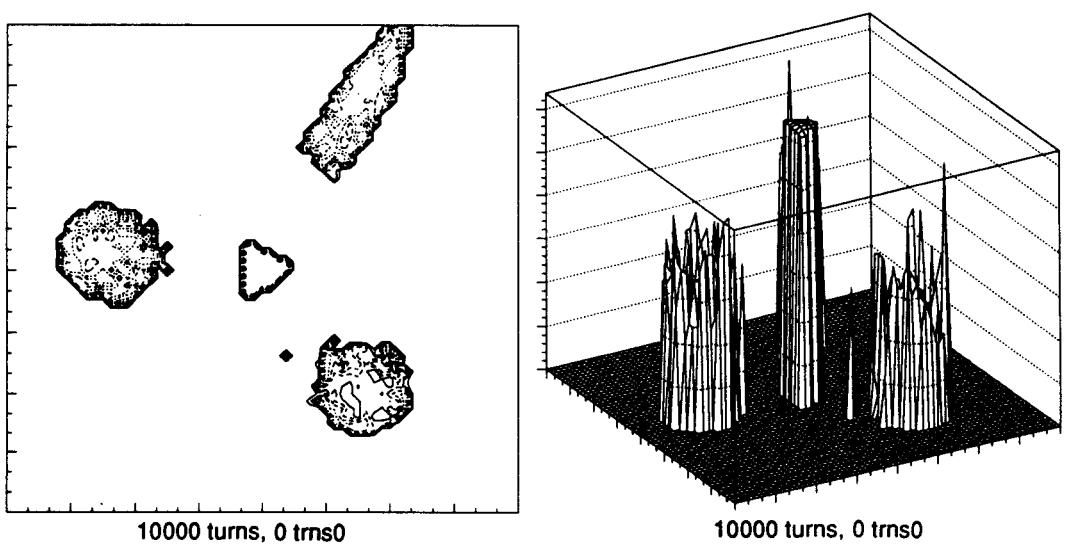

Figure 16. Sextupole combined with octupole at a beta value and tune known to produce some looping closed orbits far beyond the sextupole-alone dynamic aperture. Tune is near $\frac{1}{3}$ (0.34).

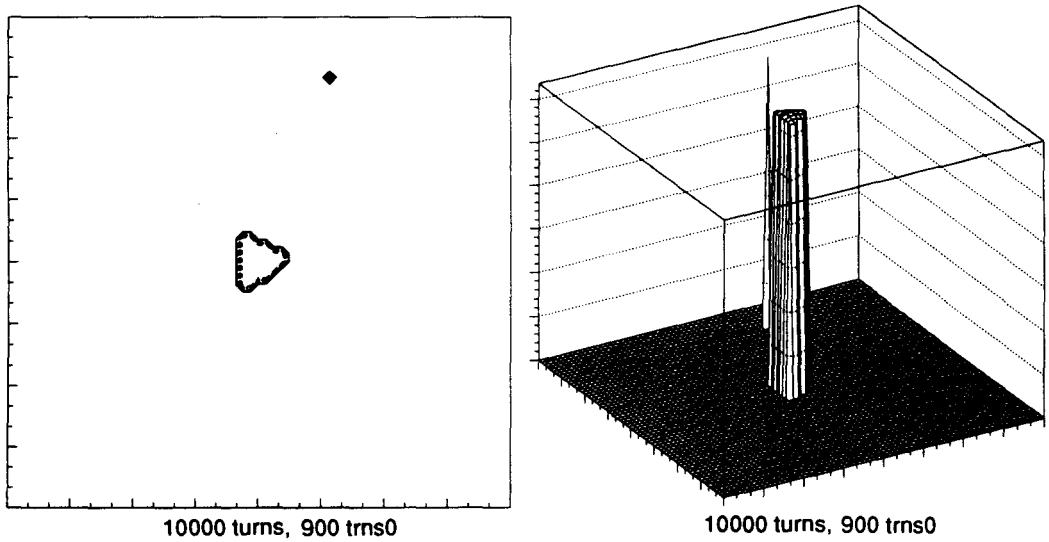

Figure 17. Same as Figure 16 except for 900-turn adiabatic ramp-up of the nonlinear kick.

Figure 18 shows the slightly distorted square dynamic aperture produced by an octupole alone at a tune close to $\frac{1}{4}$. Figure 19 shows the largely rounded-corner square contour lines within the dynamic aperture when this octupole is adiabatically ramped up over 15,000 turns.

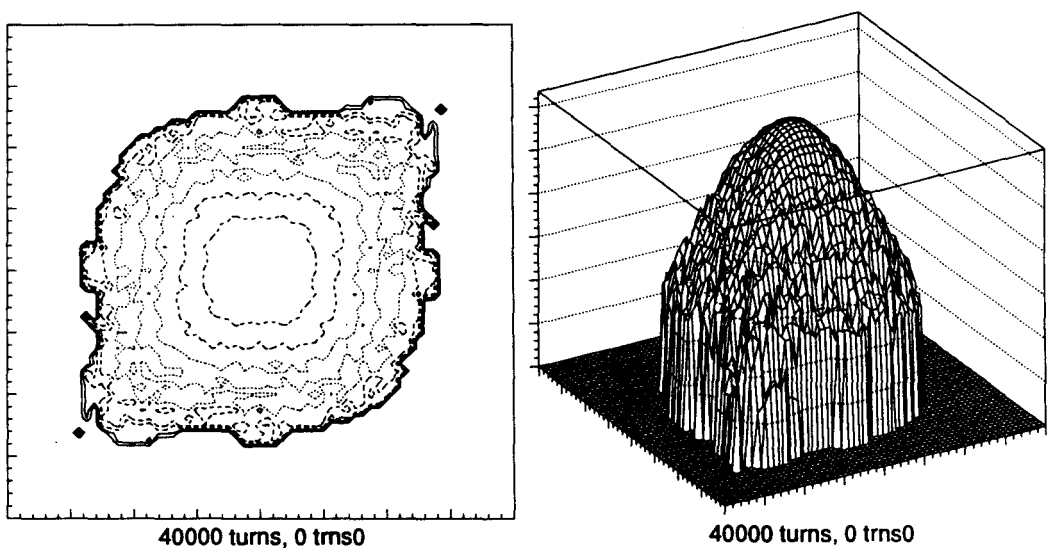

Figure 18. Octapole only with tune near $\frac{1}{4}$ (0.248).

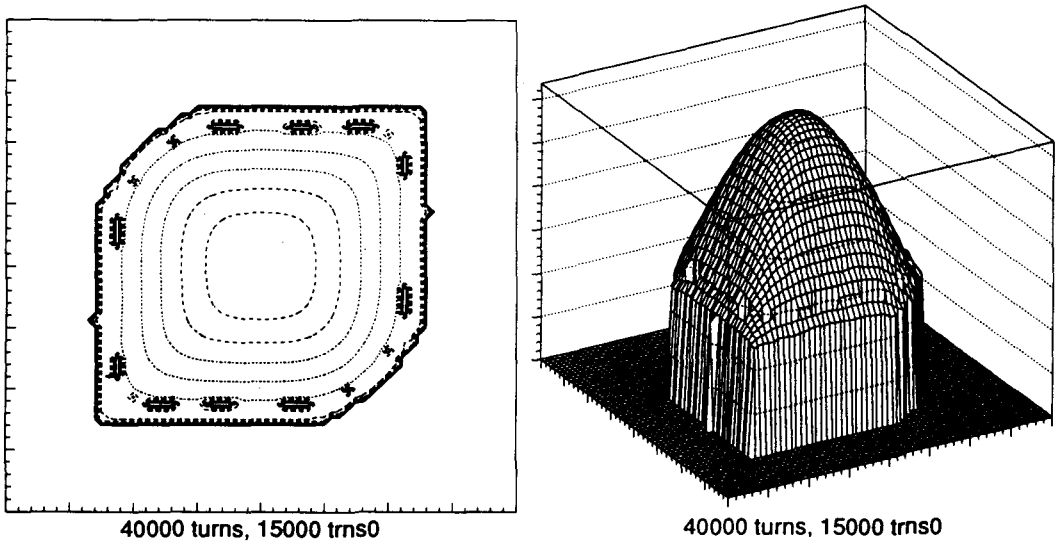

Figure 19. Same as Figure 18 except for 15,000-turn adiabatic octupole ramp-up.

Figure 20 shows a slightly distorted "five-pointed star" dynamic aperture produced by a decapole alone at a tune very near $\frac{1}{5}$. Figure 21 shows that when the decapole is adiabatically ramped up over 18,000 turns, the contours within the dynamic aperture change from being rounded-corner pentagons to being rounded corner five-pointed stars as one moves outwards. This deviation from the naively expected rounded-corner pentagon shapes no doubt reflects the significant decapole propensity for inducing amplitude dependent tune shifts.

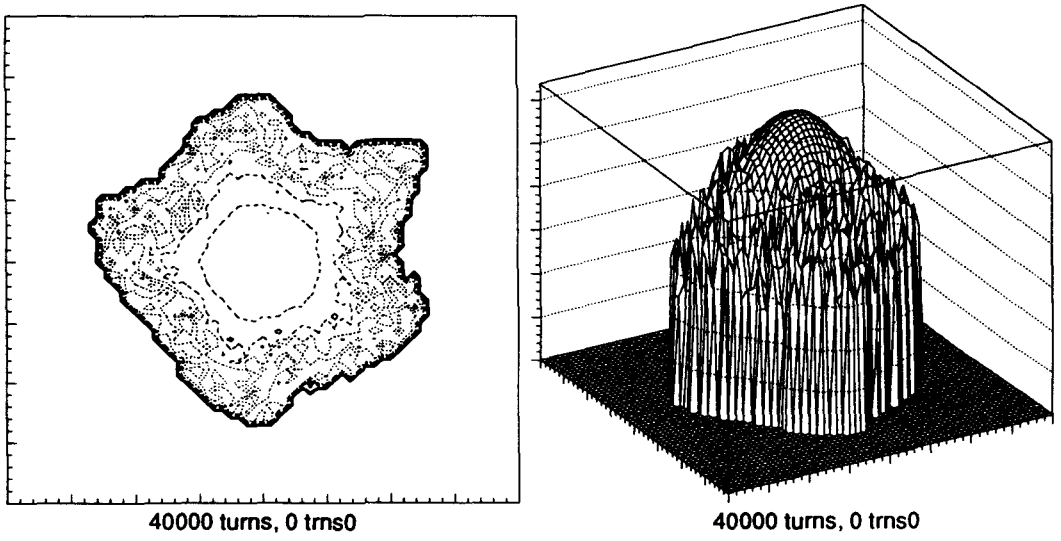

Figure 20. Decapole only with tune near $\frac{1}{5}$ (0.199).

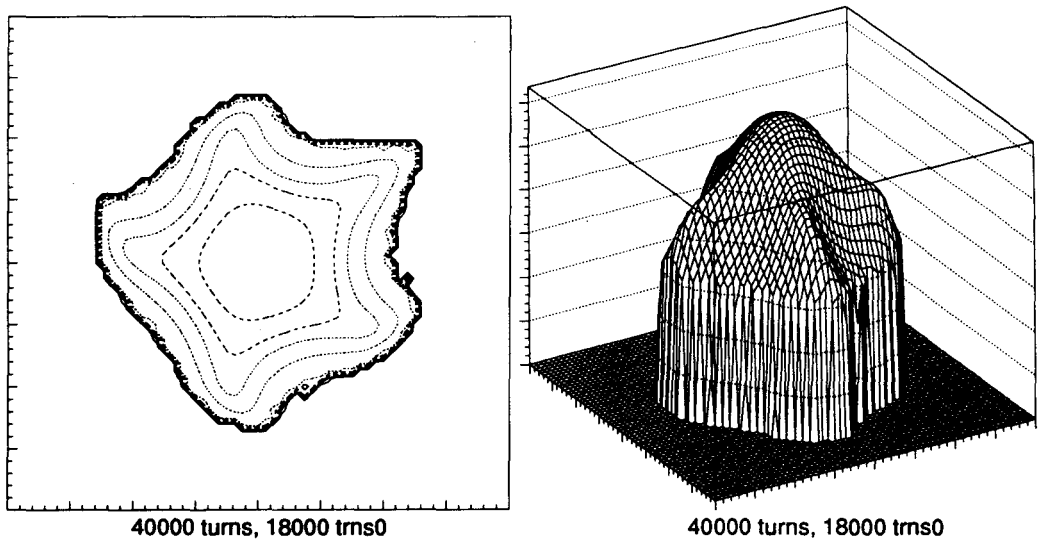

Figure 21. Same as Figure 20 except for 18,000-turn adiabatic decapole ramp-up.